The Chemistry of Monoanionic Carbaborane Ligands. Synthesis and Structure of Compounds with Carbonyl and Cycloocta-1,5-diene Ligands Additionally bound to Metal Atoms, including a Cationic Carbametallaborane†

Natalia L. Douek and Alan J. Welch*
Department of Chemistry, University of Edinburgh, Edinburgh EH9 3JJ, UK

Reaction of $[(ML_2Cl)_2]$ with $Tl[9\text{-}SMe_2\text{-}nido\text{-}7,8\text{-}C_2B_9H_{10}]$ affords the new compounds $[3,3\text{-}L_2\text{-}4\text{-}SMe_2\text{-}closo\text{-}3,1,2\text{-}MC_2B_9H_{10}]$. Compounds **1** (M = Rh, L = CO), **2** (M = Rh, $L_2 = \eta^2,\eta^2\text{-}1,5\text{-}C_8H_{12}$) and **3** (M = Pd, $L_2 = \eta^2,\sigma\text{-}5\text{-}OMe\text{-}C_8H_{12}$) were characterised by microanalysis, multinuclear NMR spectroscopy and, in the case of **1** and **2**, single-crystal X-ray diffraction studies. The experimentally determined conformations of the ML_2 fragments relative to the carbaborane ligands in **1** and **2** are in broad agreement with those predicted by analysis of the results of extended Hückel molecular orbital (EHMO) calculations on model compounds, especially in the case of **2**. Reaction of **3** with HBF_4 in diethyl ether affords the cationic heteroborane $[3\text{-}(\eta^2,\eta^2\text{-}1,5\text{-}C_8H_{12})\text{-}4\text{-}SMe_2\text{-}closo\text{-}3,1,2\text{-}PdC_2B_9H_{10}]^+$ **4**$^+$. Crystallographic study of **4**$^+BF_4^-$ reveals a molecular conformation substantially influenced by H ··· F inter-ion contacts. Comparative EHMO calculations on **2** and **4**$^+$ imply that the majority of the additional positive charge in the latter is not localised on the pendant sulfur atom alone, but rather is delocalised over the 12 cluster vertices and the atoms directly bonded to them.

Literally hundreds of transition-metal compounds of carbametallaboranes[1-3] have been prepared since the initial syntheses of $[Fe(C_2B_9H_{11})_2]^{n-}$, $n = 1$ or 2,[4] nearly 30 years ago. Of these by far the largest sub-group are compounds of the *dianionic* ligand $[C_2B_9H_{11}]^{2-}$[5] and its *C*-alkyl or -aryl derivatives. In contrast there are very few reported transition-metal compounds of *monoanionic* (or 'charge-compensated') carbaborane ligands of the general type $[LC_2B_9H_{10}]^-$ where L is a $2e^-$ function, *e.g.* pyridine, tetrahydrofuran (thf), PR_3, NCR or SR_2,[6-10] in spite of the fact that these latter ligands are more analogous to $C_5H_5^-$ the transition-metal chemistry of which is vast.[11]

We have previously prepared several transition-metal compounds of $[9\text{-}SMe_2\text{-}nido\text{-}7,8\text{-}C_2B_9H_{10}]^-$ in which the metal fragments formally contribute one[7] or three[8,9] orbitals in bonding to the carbaborane. In the present study we describe the synthesis and spectroscopic and structural characterisation of $ML_2SMe_2C_2B_9H_{10}$ compounds of palladium and rhodium, focusing on the conformation adopted by the formal two-orbital donor with respect to the carbaborane, and exploit the analogy of the carbaborane anion with $C_5H_5^-$ to synthesise an unusual example of a *cationic* carbametallaborane.

Experimental

Syntheses.—All synthetic procedures were carried out under an atmosphere of dry, oxygen-free dinitrogen using Schlenk-line techniques, with some subsequent manipulation in the open laboratory. Solvents were dried and distilled under N_2, and degassed by several freeze–pump–thaw cycles, just before use. The NMR spectra were recorded at room temperature from $CDCl_3$ or $(CD_3)_2CO$ solutions on Bruker WP200SY or WH360 spectrometers, IR spectra from CH_2Cl_2 solutions on a Perkin Elmer 598 spectrometer. Microanalyses were performed by the departmental service. The starting materials $[\{Rh(CO)_2Cl\}_2]$,[12] $[\{Rh(cod)Cl\}_2]$[13] (cod = $\eta^2,\eta^2\text{-}1,5\text{-}C_8H_{12}$), $[\{Pd(\eta^2,\sigma\text{-}5\text{-}OMe\text{-}C_8H_{12})Cl\}_2]$[14] and $Tl[9\text{-}SMe_2\text{-}nido\text{-}7,8\text{-}C_2B_9H_{10}]$[8] were made by literature methods.

$[3,3\text{-}(CO)_2\text{-}4\text{-}SMe_2\text{-}3,1,2\text{-}RhC_2B_9H_{10}]$ **1**. Solid $Tl[9\text{-}SMe_2\text{-}nido\text{-}7,8\text{-}C_2B_9H_{10}]$ (0.181 g, 0.45 mmol) was added to a frozen solution of $[\{Rh(CO)_2Cl\}_2]$ (0.081 g, 0.21 mmol) in CH_2Cl_2 (20 cm^3) and the mixture allowed to warm to room temperature with stirring. After approximately 3 h no $[\{Rh(CO)_2Cl\}_2]$ was detected by IR spectroscopy, at which point the reaction mixture was filtered through Celite and the filtrate concentrated *in vacuo* to *ca.* 1 cm^3. From this the product was isolated by thin-layer chromatography (TLC) on silica plates as a dark yellow band (R_f 0.85) upon elution with CH_2Cl_2. Crystallisation by solvent diffusion [CH_2Cl_2–hexane (1:4), −30 °C] afforded yellow-orange *plates* of $[3,3\text{-}(CO)_2\text{-}4\text{-}SMe_2\text{-}3,1,2\text{-}RhC_2B_9H_{10}]$ **1**. Yield 0.08 g (0.22 mmol, 52%) (Found: C, 21.6; H, 4.90. Calc. for $C_6H_{16}B_9O_2RhS$: C, 20.4; H, 4.60%). IR: ν_{max} at 2530 (BH), 2040 and 1990 (CO) cm^{-1}. NMR ($CDCl_3$): ^1H, δ 3.07 (br s, 1 H, cage CH), 2.94 (s, 3 H, CH_3), 2.81 (br s, 1 H, cage CH) and 2.52 (s, 3 H, CH_3); $^{11}B\text{-}\{^1H\}$, δ −6.02 [1 B, B(4)], −9.43 (3 B), −14.38 (2 B), −19.26 (1 B), −23.13 (1 B) and −25.19 (1 B).

$[3\text{-}cod\text{-}4\text{-}SMe_2\text{-}3,1,2\text{-}RhC_2B_9H_{10}]$ **2**. Similarly the reaction between $Tl[9\text{-}SMe_2\text{-}nido\text{-}7,8\text{-}C_2B_9H_{10}]$ (0.182 g, 0.46 mmol) and $[\{Rh(cod)Cl\}_2]$ (0.104 g, 0.21 mmol) in CH_2Cl_2 (10 cm^3) for 1 h afforded, after filtration, a clear yellow solution. Concentration followed by TLC yielded, on elution with CH_2Cl_2–hexane (3:2), a broad yellow band (R_f 0.50) from which was isolated a bright yellow solid. Solvent diffusion [CH_2Cl_2–hexane (1:4), −30 °C] produced both plate-like (**2α**) and columnar (**2β**) *crystals* of $[3\text{-}cod\text{-}4\text{-}SMe_2\text{-}3,1,2\text{-}RhC_2B_9H_{10}]$ **2**. Combined yield 0.108 g (0.27 mmol, 63%) (Found: C, 34.4; H, 7.35. Calc. for $C_{12}H_{28}B_9RhS$: C, 35.6; H, 7.00%). IR: ν_{max} at 2910, 2870 and 2830 (CH), and 2540 (BH) cm^{-1}. NMR ($CDCl_3$): ^1H, δ 4.42–4.38 (m, 2 H, CH), 4.21–4.19 (m, 2 H, CH), 2.98 (s, 3 H, CH_3), 2.62–2.52 (m, 4 H, CH_2), 2.53 (s, 3 H, CH_3), 2.52 (br s, 1 H, cage CH), 2.33–2.25 (m, 2 H, CH_2), 2.07–2.00 (m, 2 H, CH_2) and 1.92 (br s, 1 H, cage CH): $^{11}B\text{-}\{^1H\}$, δ −5.78 [1 B, B(4)], −7.19 (1 B), −9.99 (1 B), −12.55 (2 B),

† *Supplementary data available:* see Instructions for Authors, *J. Chem. Soc., Dalton Trans.*, 1993, Issue 1, pp. xxiii–xxviii.
Non-SI unit employed: eV ≈ 1.60 × 10^{-19} J.

Table 1 Crystal data and pertinent details of data collection and structure refinement

Compound	**1**	**2α**	**2β**	**3**	**4**$^+$**BF**$_4^-$
Formula	$C_6H_{16}B_9O_2RhS$	$C_{12}H_{28}B_9RhS$	$C_{12}H_{28}B_9RhS$	$C_{13}H_{31}B_9OPdS$	$C_{12}H_{28}B_{10}F_4PdS$
M	352.44	404.62	404.62	439.13	494.87
System	Monoclinic	Triclinic	Monoclinic	Monoclinic	Monoclinic
Space group	$P2_1/a$	$P\bar{1}$	$P2_1/c$	$P2_1/c$	$P2_1/n$
a/Å	13.1562(21)	7.0003(10)	7.163(8)	8.499(4)	9.8407(17)
b/Å	8.2858(14)	8.5300(15)	14.328(5)	14.343(3)	18.701(7)
c/Å	13.526(3)	16.315(3)	17.844(5)	16.808(5)	12.2289(22)
α/°	90	100.473(13)	90	90	90
β/°	90.333(16)	93.506(12)	92.27(5)	104.50(3)	108.750(14)
γ/°	90	107.439(13)	90	90	90
U/Å^3	1474.4	907.0	1829.9	1983.7	2131.1
Z	4	2	4	4	4
D_c/g cm^{-3}	1.587	1.481	1.468	1.470	1.542
μ(Mo-Kα)/cm^{-1}	12.59	10.26	10.17	10.22	9.82
F(000)	696	412	824	896	992
θ(orientation)/°	9–14	12–15	8–12	8–12	12–13
Data	$+h + k \pm l$	$+h \pm k \pm l$	—	—	$+h + k \pm l$
Data collection/h	55	116	—	—	132
Crystal decay (%)	3	2	—	—	0
Unique data	2923	3007	—	—	6113
Observed data	2382	2988	—	—	5148
R_{merge}	0.0568	0.0413			0.0756
U_H/Å^2	0.071(3)	0.0583(16)	—	—	0.0769(21)
g	0.001 950	0.000 159	—	—	0.000 398
Variables	209	269	—	—	314
R	0.0289	0.0212	—	—	0.0352
R'	0.0460	0.0280	—	—	0.0414
S	1.726	1.179	—	—	1.138
Maximum, minimum residue/e Å^{-3}	0.37, −0.83	0.29, −0.43	—	—	1.10, −0.95

−15.12 (1 B), −20.46 (1 B), −24.45 (1 B) and −25.49 (1 B); ^{13}C [CD_2Cl_2, DEPT (distortionless enhancement of polarisation transfer)], δ 78.31 [d, $^1J_{RhC}$ 12.1, 2 C, CH], 77.33 [d, $^1J_{RhC}$ 11.1 Hz, 2 C, CH], 34.61 (s, 2 C, CH_2), 30.25 (s, 2 C, CH_2), 28.96 (s, 1 C, CH_3) and 25.97 (s, 1 C, CH_3).

[3-(η^2,σ-5-OMe-C_8H_{12})-4-SMe_2-3,1,2-$PdC_2B_9H_{10}$] **3**. Solid Tl[9-SMe_2-*nido*-7,8-$C_2B_9H_{10}$] (0.130 g, 0.33 mmol) was added to a rapidly stirred suspension of [{Pd(η^2,σ-5-OMe-C_8H_{12})Cl}$_2$] (0.090 g, 0.16 mmol) in Me_2CO (10 cm^3) at room temperature, immediately producing a canary-yellow solution. Filtration and evaporation to dryness *in vacuo* yielded [3-(η^2,σ-5-OMe-C_8H_{12})-4-SMe_2-3,1,2-$PdC_2B_9H_{10}$] **3** as a yellow *solid*. Yield 0.101 g (0.23 mmol, 70%) (Found: C, 35.8; H, 6.95. Calc. for $C_{13}H_{31}B_9OPdS$: C, 35.6; H, 7.10%). NMR [$(CD_3)_2CO$]: ^{1}H, δ 3.18 (s, 3 H, OCH_3), 3.17 (s, 3 H, OCH_3), 2.95 (s, 3 H, SCH_3), 2.83 (s, 3 H, SCH_3), 2.56 (s, 3 H, SCH_3) and 2.51 (s, 3 H, SCH_3). Crystallisation by solvent diffusion [Me_2CO–hexane (1:4), −30 °C] afforded golden-yellow blocks from which unit-cell parameters were determined (Table 1).

[3-cod-4-SMe_2-3,1,2-$PdC_2B_9H_{10}$]BF_4 **4**$^+$$BF_4^-$. To a stirred solution of compound **3** (0.140 g, 0.32 mmol) in Et_2O (10 cm^3) at room temperature was added HBF_4·OEt_2 (55 μl of 85% solution, equivalent to 0.32 mmol), resulting in the immediate formation of an oily purple solid. This was filtered off, washed with Et_2O (3 × 5 cm^3), dissolved in CH_2Cl_2 (3 cm^3) and filtered through Celite. The resultant filtrate was overlaid with hexane (10 cm^3) and then cooled to −30 °C, resulting in the growth of diffraction-quality dark pink *plates* of [3-cod-4-SMe_2-3,1,2-$PdC_2B_9H_{10}$]BF_4. Yield 0.062 g (0.12 mmol, 39%) (Found: C, 28.7; H, 5.35. Calc. for $C_{12}H_{28}B_{10}F_4PdS$: C, 29.1; H, 5.70%). IR: ν_{max} at 2910–2830 (vbr, CH), 2540 (BH) and 1050–1010 (vbr, BF) cm^{-1}. NMR [$(CD_3)_2CO$]: ^{1}H, δ 6.32–6.23 (m, 2 H, CH), 6.17–6.06 (m, 2 H, CH), 4.60 (br s, 1 H, cage CH), 4.55 (br s, 1 H, cage CH), 3.25–3.05 (m, 4 H, CH_2), 3.02 (s, 3 H, CH_3), 2.96–2.74 (m, 4 H, CH_2) and 2.69 (s, 3 H, CH_3); ^{11}B-{^{1}H}, δ 8.37 (1 B), 1.02 (1 B, BF_4), −3.60 (2 B), −5.13 [1 B, B(4)], −8.96 (2 B), −10.10 (1 B), −14.65 (1 B) and −19.88 (1 B).

X-Ray Crystallography.—All measurements were made at ambient temperature using an Enraf-Nonius CAD4 diffractometer operating with graphite-monochromated Mo-Kα X-radiation, $\bar{\lambda}$ = 0.710 69 Å. Unit-cell parameters and orientation matrices were obtained by least-squares refinement of the setting angles of 25 strong, high-angle reflections. One asymmetric fraction of the intensity data was collected in the range $1 < \theta < 25°$ from compounds **1**, **2α** and **4**$^+$$BF_4^-$ by ω–2θ scans in 96 steps, with a ω scan width of 0.8 + 0.34 tanθ and ω scan speeds between 0.87 and 2.35° min^{-1}.

For the salt **4**$^+$$BF_4^-$ neither significant crystal decay nor movement was noted, but **1** and **2α** underwent slight decay during data collection, and net intensities were corrected accordingly. All data were corrected for Lorentz and polarisation effects using CADABS[15] and only those data for which $F > 2.0\sigma(F)$ were retained.

All three structures were solved by Patterson syntheses (metal atom) and developed by full-matrix least-squares refinement/ΔF syntheses (all other non-H atoms) using the SHELX 76 package.[16] Cage C atoms were unambiguously identified by a combination of refined (as B) isotropic thermal parameters and interatomic distances, thereby being assigned, in all cases, to stereochemically sensible positions. Cage and alkenyl H atoms were located from ΔF maps and allowed positional refinement, but methyl and methylene H atoms were introduced into idealised positions and allowed to ride on their respective C atom. All H atoms were given a (variable) group isotropic thermal parameter. An empirical absorption correction (DIFABS[17]) was applied after isotropic convergence. Therefore, equivalent data were merged, and non-H atoms refined with anisotropic thermal parameters. Data were thereafter weighted according to $w^{-1} = [\sigma^2(F) + gF^2]$. Details of crystal data and structure refinement appear in Table 1. Tables 2–4 list final coordinates of non-hydrogen atoms for compounds **1**, **2α** and **4**$^+$$BF_4^-$ respectively.

Crystallographic programs in addition to those referenced above were CALC[18] and SHELXTL.[19] Atomic scattering factors were taken from ref. 20 or inlaid in SHELX 76.

Table 2 Fractional coordinates of non-hydrogen atoms in [3,3-$(CO)_2$-4-SMe_2-*closo*-3,1,2-$RhC_2B_9H_{10}$] **1**

Atom	*x*	*y*	*z*
Rh(3)	0.434 17(2)	0.635 12(3)	0.649 35(1)
S	0.240 44(5)	0.648 37(8)	0.808 42(5)
C(1S)	0.289 1(3)	0.839 2(4)	0.846 9(3)
C(2S)	0.188 1(3)	0.576 2(5)	0.922 7(3)
C(1)	0.359 48(22)	0.401 0(3)	0.682 41(22)
C(2)	0.471 2(3)	0.359 3(3)	0.644 81(25)
B(4)	0.359 84(19)	0.526 9(3)	0.783 74(20)
B(5)	0.339 11(22)	0.316 2(4)	0.797 36(25)
B(6)	0.411 4(3)	0.210 9(4)	0.707 5(3)
B(7)	0.557 02(23)	0.470 8(4)	0.709 81(24)
B(8)	0.487 72(20)	0.575 2(3)	0.807 16(20)
B(9)	0.424 74(21)	0.419 6(3)	0.877 54(23)
B(10)	0.457 41(24)	0.227 6(4)	0.830 0(3)
B(11)	0.540 09(25)	0.256 4(4)	0.728 7(3)
B(12)	0.549 22(24)	0.388 8(4)	0.831 8(3)
C(10)	0.523 3(3)	0.799 4(4)	0.615 23(22)
O(1)	0.578 2(3)	0.898 1(3)	0.592 99(25)
C(20)	0.336 6(3)	0.730 3(6)	0.565 32(25)
O(2)	0.279 05(25)	0.791 1(6)	0.516 1(3)

Table 3 Fractional coordinates of non-hydrogen atoms in [3-(η^2,η^2-C_8H_{12})-4-SMe_2-*closo*-3,1,2-$RhC_2B_9H_{10}$] **2**

Atom	*x*	*y*	*z*
C(1)	0.304 6(3)	−0.009 8(3)	0.753 02(15)
C(2)	0.253 2(4)	0.135 9(3)	0.712 46(16)
Rh(3)	−0.007 36(3)	−0.112 86(2)	0.692 98(1)
B(4)	0.143 0(4)	−0.080 0(3)	0.822 12(16)
B(5)	0.386 9(4)	0.064 8(3)	0.858 70(18)
B(6)	0.455 7(4)	0.198 9(4)	0.787 61(20)
B(7)	0.041 4(4)	0.164 1(3)	0.744 61(19)
B(8)	−0.037 8(4)	0.027 9(3)	0.819 81(18)
B(9)	0.173 5(4)	0.096 2(3)	0.902 28(18)
B(10)	0.365 5(5)	0.269 6(3)	0.880 83(20)
B(11)	0.284 7(5)	0.311 6(4)	0.785 77(20)
B(12)	0.105 0(5)	0.245 9(3)	0.854 17(20)
S	0.114 55(10)	−0.295 00(7)	0.846 06(4)
C(1S)	−0.142 3(4)	−0.366 3(4)	0.866 97(19)
C(2S)	0.241 1(5)	−0.265 9(4)	0.949 34(19)
C(11)	−0.314 4(4)	−0.266 4(3)	0.671 42(17)
C(12)	−0.286 9(4)	−0.137 2(4)	0.625 33(18)
C(13)	−0.277 6(5)	−0.161 2(4)	0.531 83(19)
C(14)	−0.136 3(5)	−0.258 9(4)	0.501 52(17)
C(15)	0.034 6(4)	−0.235 1(3)	0.569 60(16)
C(16)	0.027 1(4)	−0.344 5(3)	0.624 75(16)
C(17)	−0.155 5(5)	−0.493 5(3)	0.626 01(19)
C(18)	−0.350 2(4)	−0.449 2(4)	0.628 93(18)

Table 4 Fractional coordinates of non-hydrogen atoms in [3-(η^2,η^2-C_8H_{12})-4-SMe_2-*closo*-3,1,2-$PdC_2B_9H_{10}$][BF_4] $\mathbf{4}^+BF_4^-$

Atom	*x*	*y*	*z*
Pd(3)	0.572 35(2)	0.376 54(1)	0.250 12(2)
C(1)	0.370 5(3)	0.412 88(18)	0.302 0(3)
C(2)	0.390 0(4)	0.469 18(19)	0.219 3(3)
B(4)	0.364 3(4)	0.325 54(19)	0.242 7(3)
B(5)	0.209 8(4)	0.372 70(22)	0.250 0(4)
B(6)	0.223 3(5)	0.464 9(3)	0.229 0(5)
B(7)	0.417 6(4)	0.426 18(24)	0.099 8(3)
B(8)	0.379 4(4)	0.331 60(24)	0.104 9(3)
B(9)	0.205 4(4)	0.326 44(25)	0.121 7(4)
B(10)	0.128 0(5)	0.412 2(3)	0.111 1(4)
B(11)	0.256 8(5)	0.475 31(25)	0.097 0(4)
B(12)	0.241 1(5)	0.389 9(3)	0.028 0(4)
S	0.405 35(9)	0.243 82(4)	0.342 10(7)
C(1S)	0.429 0(4)	0.176 86(20)	0.244 6(3)
C(2S)	0.243 8(4)	0.213 07(22)	0.362 9(4)
C(11)	0.740 2(4)	0.377 05(22)	0.167 3(3)
C(12)	0.758 7(4)	0.438 06(22)	0.231 9(4)
C(13)	0.872 2(4)	0.450 54(23)	0.348 8(4)
C(14)	0.829 3(4)	0.428 10(25)	0.451 0(4)
C(15)	0.729 8(4)	0.365 85(24)	0.430 8(3)
C(16)	0.742 1(4)	0.304 34(22)	0.377 3(3)
C(17)	0.861 0(4)	0.288 57(21)	0.326 6(3)
C(18)	0.820 8(4)	0.307 77(23)	0.199 6(3)
B	0.872 1(7)	0.120 9(3)	0.110 9(4)
F(1)	0.916 1(4)	0.120 64(16)	0.223 25(25)
F(2)	0.900 0(4)	0.056 19(13)	0.069 52(22)
F(3)	0.926 5(5)	0.172 42(17)	0.065 1(3)
F(4)	0.727 0(4)	0.133 67(20)	0.073 1(4)

Table 5 Orbital parameters used in EHMO calculations

Orbital	H_{ii}/eV	ζ_1
H(1s)	−13.60	1.30
B(2s)	−15.20	1.30
B(2p)	−8.50	1.30
C(2s)	−21.40	1.625
C(2p)	−11.40	1.625
O(2s)	−32.30	2.275
O(2p)	−14.80	2.275
S(3s)	−20.00	2.122
S(3p)	−11.00	1.827
S(3d)	−8.00	1.50
Rh(5s)	−8.61	2.135
Rh(5p)	−3.16	2.10
Rh(4d)*	−11.91	4.29

* ζ_2 1.97; coefficients in the double-ζ expansion c_1 = 0.580 95, c_2 = 0.568 24.

Additional material available from the Cambridge Crystallographic Data Centre comprises H-atom coordinates, thermal parameters and remaining bond lengths and angles.

Molecular Orbital Calculations.—To probe the frontier orbitals of the ligand an extended Hückel molecular orbital (EHMO) calculation was performed on an idealised model of the 4π electron system [9-SMe_2-*nido*-7,8-$C_2B_9H_{10}$]$^+$ constructed with B–B = B–C = C–C 1.75, B–S 1.88 and B–H = C–H 1.20 Å; SMe_2 was approximated by SH_2 (S–H 1.42 Å) with the S(lone pair)–S–B(4)–C(1) torsion angle set to 0° (employing the conventional numbering system[21] for a 4-SH_2-*closo*-1,2-dicarba-3-metallaborane). Molecular conformations for compounds **1** and **2** were probed by series of EHMO calculations on model compounds, with the $SMe_2C_2B_9H_{10}$ ligand as above and Rh–C_2B_3 plane 1.75 Å, Rh–CO 1.87, C–O 1.13 Å, CO–Rh–CO 88.5° for **1** and Rh–C_2B_3 plane 1.71, Rh–C(cod) 2.15 Å, and cod ligand from crystallographic study with C_{2v} local symmetry imposed, C–H 1.08 Å, for **2**. Orbital exponents and H_{ii} values for all these calculations are listed in Table 5.

In addition, fully charge-iterated calculations [H_{ii} = −v.s.i.e(Q), where v.s.i.e(Q) = valence-state ionisation energy of orbital i when atom has charge Q] using nine v.s.i.e.(Q) functions for Rh and Pd, two each for B, C and S, and one for H were carried out on the experimentally determined structures of compounds **2** and $\mathbf{4}^+$, except that Me was replaced by H (in the same direction) with S–H 1.42 Å, for computational expedience.

All EHMO calculations were performed using a locally modified version of ICON 8,[22] employing the modified Wolfsberg–Helmholtz formula.[23]

Results and Discussion

Compound **1**.—The reaction between [{$Rh(CO)_2Cl$}$_2$] and 2 equivalents of Tl[9-SMe_2-*nido*-7,8-$C_2B_9H_{10}$] in CH_2Cl_2 affords compound **1** in moderate yield following purification by standard chromatographic methods. It is analogous to a known

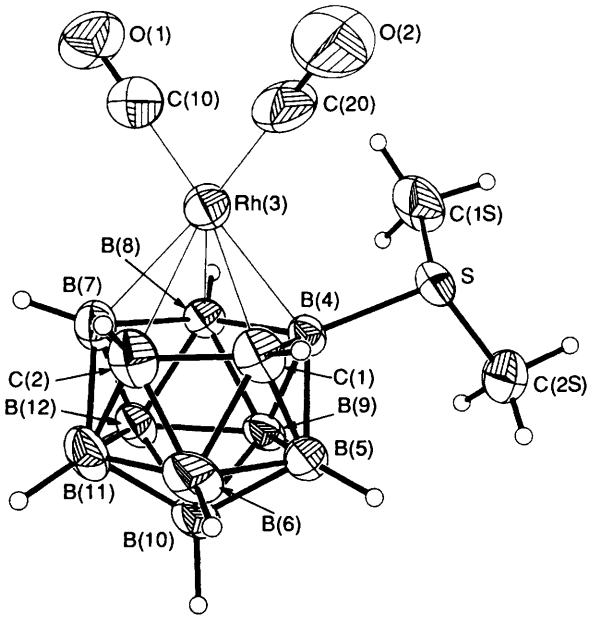

Fig. 1 Perspective view of compound **1** (50% probability ellipsoids except for H atoms). Cage H atoms carry same number as B or C to which they are bound

Table 6 Selected interatomic distances (Å) and angles (°) in [3,3-$(CO)_2$-4-SMe_2-*closo*-3,1,2-$RhC_2B_9H_{10}$] **1**

Rh(3)–C(1)	2.221(3)	B(4)–B(9)	1.766(4)
Rh(3)–C(2)	2.337(3)	B(5)–B(6)	1.777(5)
Rh(3)–B(4)	2.255(3)	B(5)–B(9)	1.779(4)
Rh(3)–B(7)	2.263(3)	B(5)–B(10)	1.775(4)
Rh(3)–B(8)	2.298(3)	B(6)–B(10)	1.767(5)
Rh(3)–C(10)	1.857(3)	B(6)–B(11)	1.756(5)
Rh(3)–C(20)	1.883(4)	B(7)–B(8)	1.824(4)
S–C(1S)	1.782(4)	B(7)–B(11)	1.809(5)
S–C(2S)	1.799(4)	B(7)–B(12)	1.788(5)
S–B(4)	1.897(3)	B(8)–B(9)	1.807(4)
C(1)–C(2)	1.596(4)	B(8)–B(12)	1.774(4)
C(1)–B(4)	1.723(4)	B(9)–B(10)	1.770(4)
C(1)–B(5)	1.728(4)	B(9)–B(12)	1.772(4)
C(1)–B(6)	1.749(5)	B(10)–B(11)	1.771(5)
C(2)–B(6)	1.690(5)	B(10)–B(12)	1.801(5)
C(2)–B(7)	1.700(5)	B(11)–B(12)	1.778(5)
C(2)–B(11)	1.681(5)	C(10)–O(1)	1.133(4)
B(4)–B(5)	1.777(4)	C(20)–O(2)	1.125(6)
B(4)–B(8)	1.756(4)		
C(1)–Rh(3)–C(2)	40.88(11)	B(7)–Rh(3)–C(10)	94.59(13)
C(1)–Rh(3)–B(4)	45.26(10)	B(7)–Rh(3)–C(20)	162.43(15)
C(1)–Rh(3)–C(10)	166.19(13)	B(8)–Rh(3)–C(10)	101.45(12)
C(1)–Rh(3)–C(20)	100.74(14)	B(8)–Rh(3)–C(20)	148.81(14)
C(2)–Rh(3)–B(7)	43.34(11)	C(10)–Rh(3)–C(20)	88.42(16)
C(2)–Rh(3)–C(10)	125.32(13)	S–B(4)–C(1)	117.58(18)
C(2)–Rh(3)–C(20)	122.35(14)	S–B(4)–B(5)	112.04(17)
B(4)–Rh(3)–B(8)	45.37(10)	S–B(4)–B(8)	129.84(18)
B(4)–Rh(3)–C(10)	140.29(12)	S–B(4)–B(9)	122.57(18)
B(4)–Rh(3)–C(20)	110.84(14)	Rh(3)–C(10)–O(1)	178.8(3)
B(7)–Rh(3)–B(8)	47.14(11)	Rh(3)–C(20)–O(2)	178.1(4)

synthesis of $[Rh(CO)_2(C_5Me_5)]$ [24] and is conveniently followed by IR spectroscopy, whereupon the CO stretches due to $[\{Rh(CO)_2Cl\}_2]$ at 2095 and 2030 cm^{-1} gradually give way to those due to the new product at 2040 and 1990 cm^{-1}. The appearance of a broad, strong peak centred on 2530 cm^{-1} attributable to B–H stretching modes was further testimony to the progress of the reaction. The ^1H NMR spectrum exhibits a broad signal due to each of the cage CH protons, and confirmed the magnetic inequivalence of the sulfur-bound

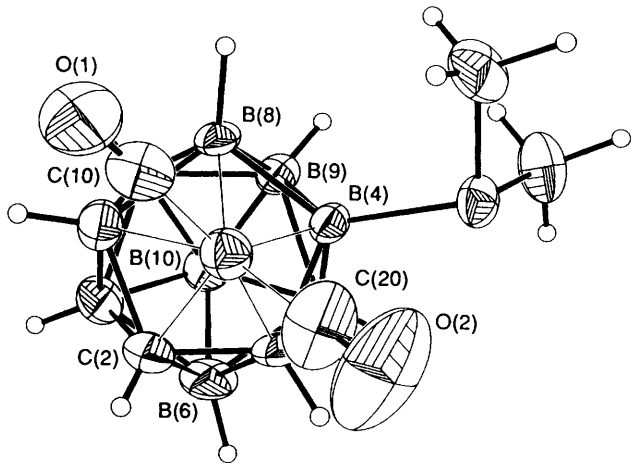

Fig. 2 Plan view of compound **1** showing the orientation of the $Rh(CO)_2$ unit with respect to the carbaborane ligand

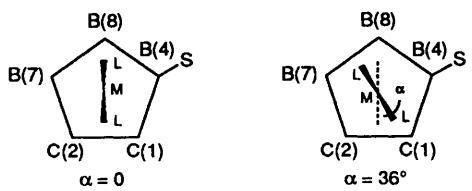

Fig. 3 Definition of the conformation angle α in $ML_2SMe_2C_2B_9H_{10}$ compounds

methyl groups.[7–10,25] The ^{11}B-$\{^1H\}$ NMR spectrum displayed six signals in the ratio (high frequency to low frequency) 1:3:2:1:1:1. On retention of proton coupling all except that at highest frequency [which may therefore be assigned to the sulfur-bearing boron atom B(4)] are split into doublets, with $^1J_{BH}$ in the range 145–161 Hz.

Whilst these data are consistent with the proposed formulation of compound **1** a single-crystal diffraction study was necessary unequivocally to establish the molecular structure and conformation. Fig. 1 presents a perspective view of a single molecule, and Table 6 lists selected interatomic distances and angles. Regarding **1** as a heteroborane, the observed *closo*-icosahedral geometry of the cage is fully consistent with electron-counting rules,[26] if one assumes a formal oxidation state for the Rh atom of +1. The metallabonded C_2B_3 polyhedral face is nearly planar [$\sigma_{C_2B_3}$ = 0.072 Å, where $\sigma = (\Sigma z_i^2)^{\frac{1}{2}}$, z_i being the displacement of the ith atom from the appropriate least-squares plane] and parallel (dihedral angle 1.42°) to the lower B(5)B(6)B(9)B(11)B(12) pentagon (σ_{B_5} = 0.044 Å). The Rh–B distances span the range 2.26–2.30 Å, but the two Rh–C_{cage} bond lengths are substantially different from each other, Rh(3)–C(2) being more than 0.1 Å longer than Rh(3)–C(1). Nevertheless, the 'slip'[27] of the metal atom across the C_2B_3 ligand face, Δ, is only 0.08 Å, in a direction away from C(2).

Fig. 2, a plan view of the molecule, clearly shows that the conformation of the $\{Rh(CO)_2\}$ fragment relative to the metallabonded C_2B_3 face is such that the $Rh(CO)_2$ plane lies essentially perpendicular to a plane through C(2), B(10) and B(9). We will describe conformations in $ML_2SMe_2C_2B_9H_{10}$ compounds by α, defined as the angle between the B(6)B(8)B(10) and ML_2 planes, with a positive value denoting anticlockwise rotation of L towards B(4), see Fig. 3. In compound **1** the experimentally determined α is 49.9°, and we have attempted to understand this conformation by consideration of the frontier MOs of $[9\text{-}SMe_2\text{-}nido\text{-}7,8\text{-}C_2B_9H_{10}]^+$ and the $\{Rh(CO)_2\}^-$ fragment. The latter, by analogy with those of $\{Pt(PH_3)_2\}$,[28] consist of a lowest unoccupied molecular orbital (LUMO) of a_1 symmetry, a highest occupied molecular orbital (HOMO, b_2) which is a d_{yz}–p_y hybrid orbital directed towards the carbaborane ligand, and a second HOMO (b_1) of d_{xz}

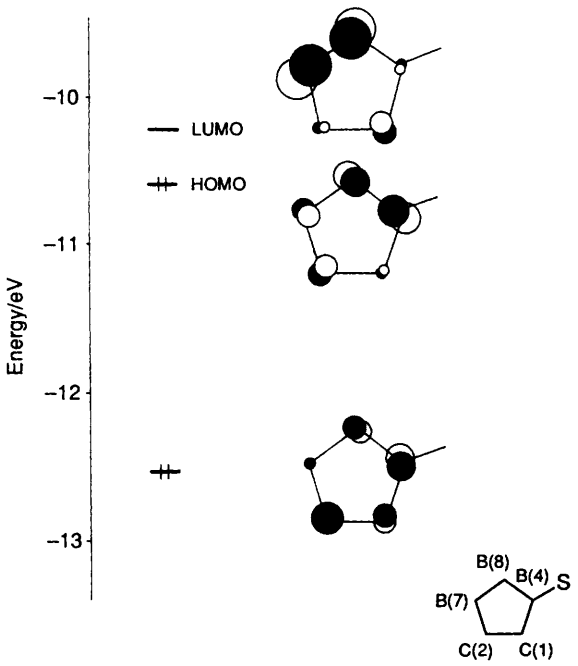

Fig. 4 The frontier π MOs of [9-SMe_2-*nido*-7,8-$C_2B_9H_{10}$]$^+$. Only those contributions of the facial atoms of the ligand are drawn

character. The frontier π MOs of [9-SMe_2-*nido*-7,8-$C_2B_9H_{10}$]$^+$ are reproduced[8] in Fig. 4. Previous analysis[27,28] of the conformations of bis(phosphine)carbaplatinaboranes has shown that the overall molecular conformation is set by the metal fragment HOMO–cage LUMO interaction. In [9-SMe_2-*nido*-7,8-$C_2B_9H_{10}$]$^+$ the nodal plane of the LUMO lies perpendicular to the ligand face and is oriented such that it cuts the C(2)–B(7) and B(4)–B(8) connectivities close to C(2) and B(4), lying parallel to B(7)–B(8). Therefore, a value of α of around 36° is anticipated; indeed, a plot of relative molecular energy *versus* α in the model compound (Fig. 5) shows a shallow minimum centred on 30°. The crystallographically observed conformation (arrowed) is barely destabilised relative to this minimum, and therefore may reflect the influence of packing forces on molecular conformation in this particular case. Indeed in the crystal structure determined one of the carbonyl oxygen atoms, O(2), lies only 2.43(4) Å from H(1) of an adjacent molecule (symmetry operation $\frac{1}{2} - x, \frac{1}{2} + y, 1 - z$).

As noted, the metal atom in compound **1** is barely slipped. Although compounds of the type $M(CO)_2$(carbaborane) have been reported previously,[29] the present study represents, as far as we are aware, the first structural characterisation of such a species. The small slip parameter observed continues the trend previously established[30] from 3-tmen-3,1,2-$PdC_2B_9H_{11}$ (Δ = 0.52 Å, tmen = *N*,*N*,*N*′,*N*′-tetramethylethylenediamine) to 3,3-$(PMe_3)_2$-3,1,2-$PdC_2B_9H_{11}$ (Δ = 0.26 Å) of reducing slip with increasing π-acceptor properties of the exopolyhedral ligand set.* The bond Rh–C(10) is significantly shorter than Rh–C(20), 0.026(5) Å, reflecting the greater *trans* influence of boron over carbon in carbaboranes generally, and 9-SMe_2-*nido*-7,8-$C_2B_9H_{10}$ specifically, since the ligand π-MOs are concentrated on the facial boron atoms.

In metal compounds of $SMe_2C_2B_9H_{10}$ that have been studied crystallographically[7–9] the S(lone pair)–S–B(4)–C(1) torsion angle, τ, is generally found to be small (so long as this produces no severe intramolecular crowding), and S–B(4)–C(1) is generally substantially less than S–B(4)–B(8); we have tentatively ascribed these stereochemical features to an H(1)$^{\delta+}$ ··· S(lone pair) bonding interaction. In **1** the measured torsion

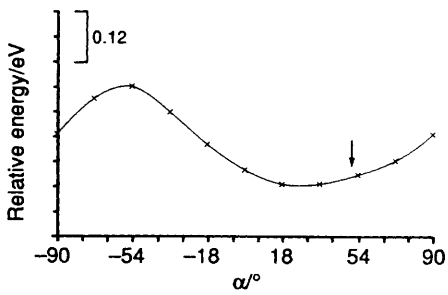

Fig. 5 Plot of relative molecular energy *versus* α for the theoretical model of compound **1**. The experimentally observed conformation is arrowed

is −13.10°, negative τ denoting a clockwise rotation of the SMe_2 group for the enantiomer shown in Fig. 1 when viewed along the S–B(4) vector, falling within the range previously determined,[7–9,25] and the difference between the aforementioned angles is 12.3°.

Compound **2**.—When [{Rh(cod)Cl}$_2$] is allowed to react with 2 equivalents of Tl[9-SMe_2-*nido*-7,8-$C_2B_9H_{10}$] in CH_2Cl_2 the bright yellow compound **2** is produced in reasonable yield, in an analogous reaction to that affording [Rh(cod)(C_5H_5)].[31] The ^{11}B-{^{1}H} NMR spectrum is broadly similar to that of **1** (except for slight differences due to coincident peaks) and is fully consistent with an asymmetric carbametallaborane. Again, the ^{11}B resonance at highest frequency is that due to the SMe_2-substituted boron atom, with all other resonances displaying doublet coupling (150–175 Hz) in the ^{11}B NMR spectrum.

Assuming that compound **2** has the same molecular architecture as **1**, except that $(CO)_2$ is replaced by cod, one might anticipate increased electron density to be associated with the cluster. It is of interest that this additional charge appears not to be localised on the nine boron nuclei (from the close similarity of the ^{11}B chemical shifts of **1** and **2**). However, some indication that it may be associated with 'second sphere' nuclei is afforded by the recognition that cage CH resonances in the ^{1}H NMR spectrum of **2** are, on average, 0.7 ppm to low frequency of those of **1**. The ^{13}C NMR spectrum of compound **2** in CD_2Cl_2 displays clear resonances due to CH_3 (SMe_2), CH_2 (cod) and CH (cod) with the last showing one-bond coupling to ^{103}Rh. The observation of only two CH_2 and two CH signals is fully consistent with rapid rotation of the cod ligand about the metal–cage axis in solution at room temperature.

Diffraction-quality crystals of compound **2** in two modifications, **2α** and **2β**, were grown by solvent diffusion. On the basis of molecular volumes measured at the same temperature (Table 1) the α form is slightly better packed, and a full set of intensity data was recorded from this form only. Table 7 lists selected interatomic distances and angles, and Figs. 6 and 7, respectively, show perspective and plan views of the compound (the latter with H atoms omitted for clarity). Like compound **1**, **2** is an essentially icosahedral *closo*-carbarhodaborane.

The angle α [calculated using the midpoints of C(11)–C(12) and C(15)–C(16)] is 27.4°, in better agreement with that predicted for $ML_2SMe_2C_2B_9H_{10}$ compounds than in **1**. Fig. 8 plots relative energy *versus* α for the theoretical model of **2**, and is drawn to the same scale as Fig. 5. Clearly the global minimum occurs at about the same α value as that predicted for **1**. However, because of intramolecular crowding between alkenyl H atoms and the SH_2 group which is maximised at α −24 and 90°, this minimum lies in a substantially deeper well, suggesting that the stereochemistry adopted in **2** is less likely to be influenced by (weak) intermolecular forces.

In compound **2** Δ is 0.09 Å, τ is −21.2°, and S–B(4)–C(1) is 10.4° less than S–B(4)–B(8), all similar to the corresponding values of **1**. The two alkene functions do not bond evenly to Rh(3), which also recalls the situation in **1**. Specifically, Rh–C(cod) distances *trans* to boron are *ca.* 0.05 Å longer than

* An additional factor contributing to the small slip in compound **1** may be the smaller d–p valence orbital gap in Rh^+, *cf.* Pd^{2+}.

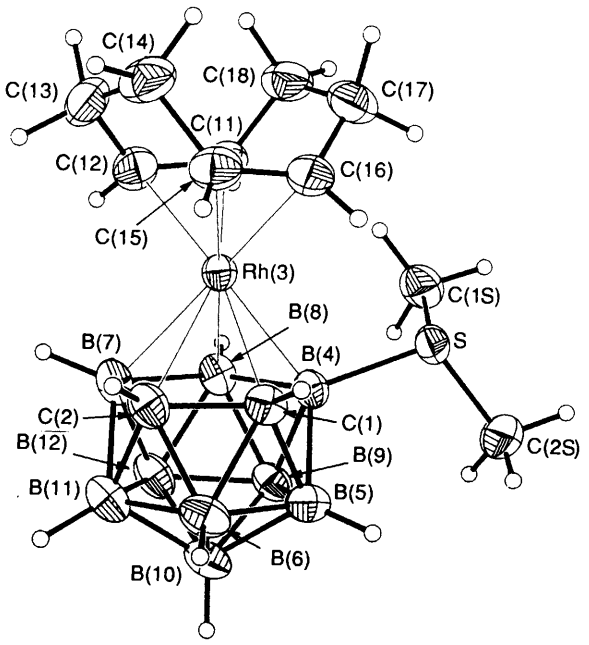

Fig. 6 Perspective view of compound **2**, with thermal ellipsoids and H-atom labelling as in Fig. 1

Table 7 Selected interatomic distances (Å) and angles (°) in [3-(η^2,η^2-C_8H_{12})-4-SMe_2-*closo*-3,1,2-$RhC_2B_9H_{10}$] **2**

C(1)–C(2)	1.628(4)	B(6)–B(10)	1.758(4)
C(1)–Rh(3)	2.1854(24)	B(6)–B(11)	1.748(4)
C(1)–B(4)	1.704(4)	B(7)–B(8)	1.838(4)
C(1)–B(5)	1.723(4)	B(7)–B(11)	1.790(4)
C(1)–B(6)	1.743(4)	B(7)–B(12)	1.773(4)
C(2)–Rh(3)	2.301(3)	B(8)–B(9)	1.814(4)
C(2)–B(6)	1.701(4)	B(8)–B(12)	1.792(4)
C(2)–B(7)	1.672(4)	B(9)–B(10)	1.781(4)
C(2)–B(11)	1.686(4)	B(9)–B(12)	1.778(4)
Rh(3)–B(4)	2.228(3)	B(10)–B(11)	1.752(4)
Rh(3)–B(7)	2.273(3)	B(10)–B(12)	1.790(4)
Rh(3)–B(8)	2.252(3)	B(11)–B(12)	1.766(4)
Rh(3)–C(11)	2.124(3)	S–C(1S)	1.793(3)
Rh(3)–C(12)	2.122(3)	S–C(2S)	1.794(4)
Rh(3)–C(15)	2.172(3)	C(11)–C(12)	1.418(4)
Rh(3)–C(16)	2.172(3)	C(11)–C(18)	1.525(4)
B(4)–B(5)	1.772(4)	C(12)–C(13)	1.510(4)
B(4)–B(8)	1.776(4)	C(13)–C(14)	1.523(5)
B(4)–B(9)	1.753(4)	C(14)–C(15)	1.522(4)
B(4)–S	1.899(3)	C(15)–C(16)	1.401(4)
B(5)–B(6)	1.762(4)	C(16)–C(17)	1.513(4)
B(5)–B(9)	1.763(4)	C(17)–C(18)	1.522(4)
B(5)–B(10)	1.772(4)		
B(7)–Rh(3)–C(11)	114.45(11)	C(1)–Rh(3)–C(16)	94.91(10)
B(7)–Rh(3)–C(12)	90.59(11)	C(2)–Rh(3)–B(7)	42.87(10)
B(7)–Rh(3)–C(15)	129.04(11)	C(2)–Rh(3)–C(11)	155.18(10)
B(7)–Rh(3)–C(16)	162.16(11)	C(2)–Rh(3)–C(12)	119.49(10)
B(8)–Rh(3)–C(11)	93.79(11)	C(2)–Rh(3)–C(15)	100.12(10)
B(8)–Rh(3)–C(12)	100.53(11)	C(2)–Rh(3)–C(16)	120.22(10)
B(8)–Rh(3)–C(15)	176.65(11)	B(4)–Rh(3)–B(8)	46.70(10)
B(8)–Rh(3)–C(16)	144.80(10)	B(4)–Rh(3)–C(11)	114.44(10)
C(11)–Rh(3)–C(12)	39.01(11)	B(4)–Rh(3)–C(12)	142.60(10)
C(15)–Rh(3)–C(16)	37.63(10)	B(4)–Rh(3)–C(15)	133.42(10)
C(1)–B(4)–S	118.93(17)	B(4)–Rh(3)–C(16)	104.21(10)
B(5)–B(4)–S	112.40(17)	B(7)–Rh(3)–B(8)	47.94(11)
B(8)–B(4)–S	129.37(18)	C(11)–C(12)–C(13)	124.8(3)
B(9)–B(4)–S	121.53(18)	C(12)–C(13)–C(14)	113.4(3)
C(1)–Rh(3)–C(2)	42.45(9)	C(13)–C(14)–C(15)	111.8(3)
C(1)–Rh(3)–B(4)	45.43(9)	C(14)–C(15)–C(16)	123.5(3)
C(1)–Rh(3)–C(11)	157.91(10)	C(15)–C(16)–C(17)	123.7(3)
C(1)–Rh(3)–C(12)	161.94(10)	C(16)–C(17)–C(18)	113.1(3)
C(1)–Rh(3)–C(15)	100.72(10)	C(11)–C(18)–C(17)	112.43(25)

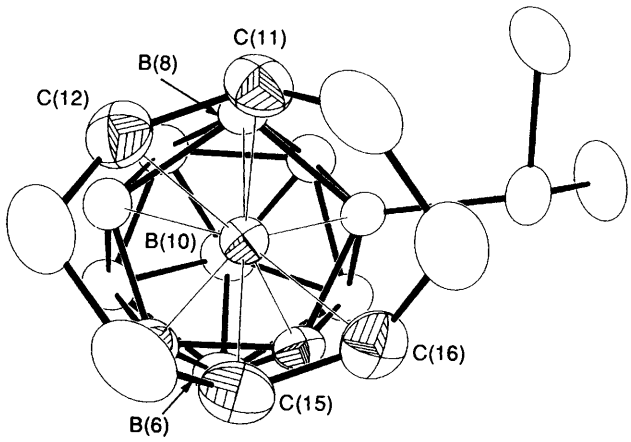

Fig. 7 Plan view of compound **2**, showing the molecular conformation. For clarity H atoms are omitted and only Rh and those carbon atoms directly bonded to it are drawn as shaded

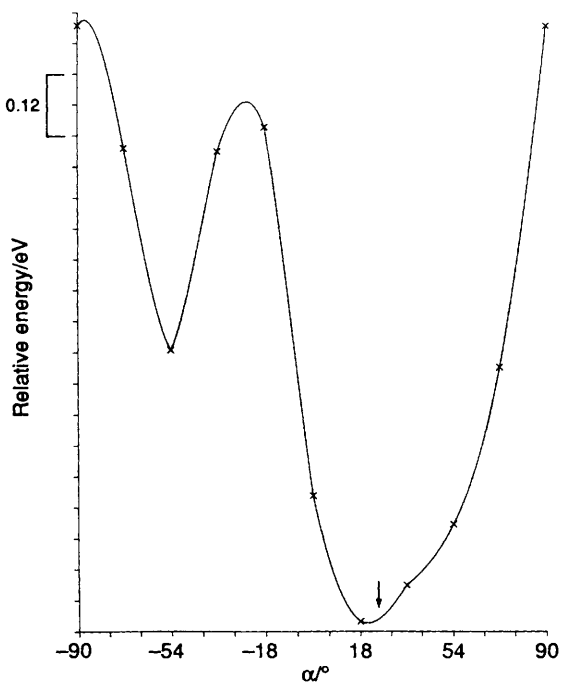

Fig. 8 Plot of relative molecular energy *versus* α for the theoretical model of compound **2**. The experimentally observed conformation is arrowed

those *trans* to (cage) carbon. Moreover, the C(15)–C(16) moiety clearly retains more alkene character than does C(11)–C(12), as evidenced by (*i*) a shorter C–C bond distance, by 0.017 Å and (*ii*) less rehybridisation at the carbon centres, one measure of which is the dihedral angle between adjacent planes through atoms $C_{CH_2}C_{CH}H$, being *ca.* 144° for C(15)–C(16) and *ca.* 134° for C(11)–C(12).

Compounds **3** *and* $\mathbf{4}^+$.—When suspensions of Tl[9-SMe_2-*nido*-7,8-$C_2B_9H_{10}$] and [{$Pd(\eta^2,\sigma$-5-OMe-C_8H_{12})Cl}$_2$] in acetone are allowed to react [14] a yellow solution of compound **3** immediately forms. In principle **3** should exist as a mixture of two geometrical isomers, differing in the position of substitution of the OMe group on the cod ligand relative to the (asymmetric) carbaborane cage. The observation in the ^1H NMR spectrum of signals tentatively assigned to two distinct OMe and four distinct SMe functions is in agreement with the existence of such isomers and implies that the C_8H_{12}(OMe) ligand remains bound to the metal centre in solution.

The treatment of compound **3** with HBF_4 [14] results in an

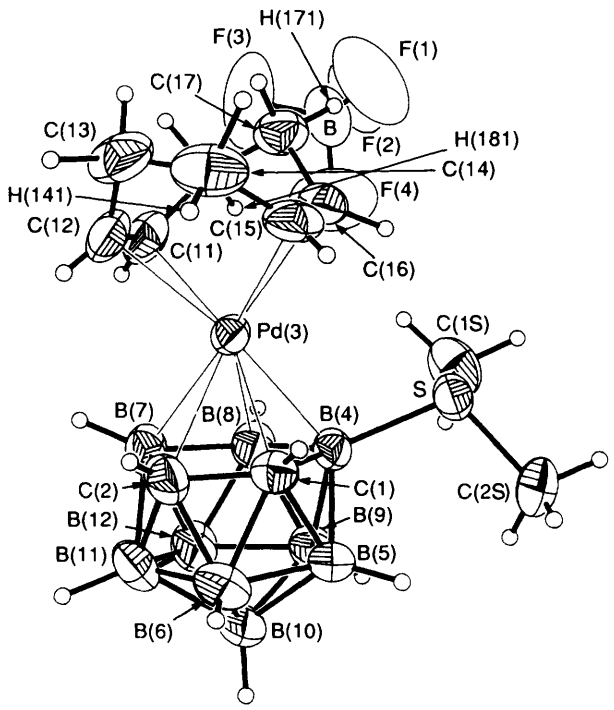

Fig. 9 Perspective view of the cation 4^+ together with the nearest BF_4^- anion. Thermal ellipsoids and cage H labels as in Fig. 1. Note that C(18) is totally obscured by C(14)

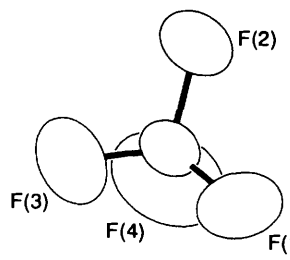

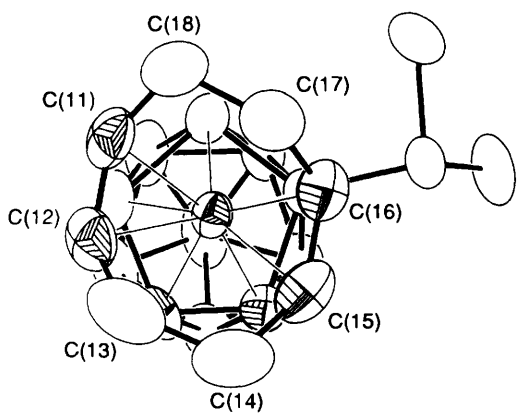

Fig. 10 Plan view of the ion pair $4^+BF_4^-$. For clarity all H atoms are omitted and only the metal atom and those carbon atoms directly bonded to it are drawn as shaded ellipsoids

immediate colour change from yellow to purple, and the dark pink solid $4^+BF_4^-$ is isolated in moderate yield following work-up. Microanalytical and IR spectroscopic data on this product are consistent with the proposed formulation. In the ^1H NMR spectrum resonances due to SMe_2, cod and cage CH protons are observed in the correct integral ratios, all moved to high frequency relative to equivalent protons in **2**, especially

Table 8 Selected interatomic distances (Å) and angles (°) in [3-(η^2,η^2-C_8H_{12})-4-SMe_2-*closo*-3,1,2-$PdC_2B_9H_{10}$][BF_4] $4^+BF_4^-$

Pd(3)–C(1)	2.371(4)	B(7)–B(8)	1.814(6)
Pd(3)–C(2)	2.434(4)	B(7)–B(11)	1.821(7)
Pd(3)–B(4)	2.234(4)	B(7)–B(12)	1.808(6)
Pd(3)–B(7)	2.181(4)	B(8)–B(9)	1.792(6)
Pd(3)–B(8)	2.301(4)	B(8)–B(12)	1.762(6)
Pd(3)–C(11)	2.198(4)	B(9)–B(10)	1.763(7)
Pd(3)–C(12)	2.236(4)	B(9)–B(12)	1.762(7)
Pd(3)–C(15)	2.263(4)	B(10)–B(11)	1.780(7)
Pd(3)–C(16)	2.316(4)	B(10)–B(12)	1.781(7)
C(1)–C(2)	1.515(5)	B(11)–B(12)	1.789(7)
C(1)–B(4)	1.780(5)	S–C(1S)	1.795(4)
C(1)–B(5)	1.681(5)	S–C(2S)	1.784(4)
C(1)–B(6)	1.735(6)	C(11)–C(12)	1.366(6)
C(2)–B(6)	1.684(7)	C(11)–C(18)	1.504(6)
C(2)–B(7)	1.763(6)	C(12)–C(13)	1.524(6)
C(2)–B(11)	1.645(6)	C(13)–C(14)	1.501(6)
B(4)–B(5)	1.784(6)	C(14)–C(15)	1.490(6)
B(4)–B(8)	1.743(6)	C(15)–C(16)	1.348(5)
B(4)–B(9)	1.774(6)	C(16)–C(17)	1.519(5)
B(4)–S	1.913(4)	C(17)–C(18)	1.518(6)
B(5)–B(6)	1.755(7)	B–F(1)	1.301(7)
B(5)–B(9)	1.780(6)	B–F(2)	1.373(6)
B(5)–B(10)	1.788(7)	B–F(3)	1.312(7)
B(6)–B(10)	1.749(7)	B–F(4)	1.373(7)
B(6)–B(11)	1.759(7)		
C(1)–Pd(3)–C(2)	36.72(12)	B(8)–Pd(3)–C(15)	148.99(15)
C(1)–Pd(3)–B(4)	43.36(13)	B(8)–Pd(3)–C(16)	122.91(14)
C(1)–Pd(3)–C(11)	160.16(14)	C(11)–Pd(3)–C(12)	35.88(15)
C(1)–Pd(3)–C(12)	131.59(14)	C(15)–Pd(3)–C(16)	34.22(14)
C(1)–Pd(3)–C(15)	97.67(13)	C(1)–B(4)–S	120.11(23)
C(1)–Pd(3)–C(16)	118.24(13)	B(5)–B(4)–S	111.89(23)
C(2)–Pd(3)–B(7)	44.49(15)	B(8)–B(4)–S	126.87(25)
C(2)–Pd(3)–C(11)	123.44(14)	B(9)–B(4)–S	119.16(24)
C(2)–Pd(3)–C(12)	101.85(14)	C(12)–C(11)–C(18)	127.4(4)
C(2)–Pd(3)–C(15)	116.95(14)	C(11)–C(12)–C(13)	126.3(4)
C(2)–Pd(3)–C(16)	148.83(13)	C(12)–C(13)–C(14)	114.9(4)
B(4)–Pd(3)–B(8)	45.16(14)	C(13)–C(14)–C(15)	115.2(4)
B(4)–Pd(3)–C(11)	142.95(14)	C(14)–C(15)–C(16)	126.2(4)
B(4)–Pd(3)–C(12)	170.40(14)	C(15)–C(16)–C(17)	124.4(3)
B(4)–Pd(3)–C(15)	109.43(14)	C(16)–C(17)–C(18)	113.0(3)
B(4)–Pd(3)–C(16)	103.43(13)	C(11)–C(18)–C(17)	114.5(3)
B(7)–Pd(3)–B(8)	47.63(16)	F(1)–B–F(2)	110.3(4)
B(7)–Pd(3)–C(11)	91.97(16)	F(1)–B–F(3)	114.3(5)
B(7)–Pd(3)–C(12)	93.99(16)	F(1)–B–F(4)	108.3(5)
B(7)–Pd(3)–C(15)	158.99(15)	F(2)–B–F(3)	109.4(4)
B(7)–Pd(3)–C(16)	166.27(15)	F(2)–B–F(4)	109.8(4)
B(8)–Pd(3)–C(11)	101.65(15)	F(3)–B–F(4)	104.6(5)
B(8)–Pd(3)–C(12)	127.62(15)		

Table 9 Inter-ion contacts of type A–B · · · C–D in [3-(η^2,η^2-C_8H_{12})-4-SMe_2-*closo*-3,1,2-$PdC_2B_9H_{10}$][BF_4] $4^+BF_4^-$

B	C	B · · · C/Å	A–B · · · C/°	B · · · C–D/°
H(171)	F(1)	2.59	141	121
H(181)	F(4)	2.66	145	94
H(141)	F(2′)	2.29	147	118
H(2)	F(2′)	2.54	142	99
H(1)	F(2″)	2.36	157	106

F(2′) refers to F(2) at $\frac{3}{2} - x, y - \frac{1}{2}, \frac{1}{2} - z$, F(2″) to F(2) at $\frac{1}{2} + x, \frac{1}{2} - y, \frac{1}{2} + z$.

cod CH and cage CH. Similarly the ^{11}B NMR signals of $4^+BF_4^-$, although not assigned, clearly appear as a group at higher frequency than those of **2**.

Thus compound 4^+ appears to be an unusual example of a *cationic* heteroborane,[31] the rarity of which justified full structural characterisation by X-ray diffraction. In Figs. 9 and 10 are presented perspective and plan views, respectively, of the cation 4^+ together with its closest BF_4^- anion, and Table 8

Table 10 Comparison of optimised atomic charges in compounds **2** and 4^+

Atom	2	4^+	Difference	Atom	2	4^+	Difference
M	0.221	0.294	0.073	S	0.345	0.357	0.012
C(1)	−0.009	0.016	0.025	H(1S)	0.082	0.085	0.003
C(2)	−0.026	−0.004	0.022	H(2S)	0.078	0.084	0.006
B(4)	0.108	0.132	0.024	C(11)	−0.041	0.019	0.060
B(5)	0.060	0.097	0.037	C(12)	−0.042	0.009	0.051
B(6)	0.091	0.115	0.024	C(13)	0.001	0.024	0.023
B(7)	0.021	0.081	0.060	C(14)	0.000	0.029	0.029
B(8)	−0.009	0.006	0.015	C(15)	−0.041	0.006	0.047
B(9)	0.013	0.041	0.028	C(16)	−0.038	0.010	0.048
B(10)	0.021	0.049	0.028	C(17)	0.002	0.019	0.017
B(11)	0.052	0.097	0.045	C(18)	−0.001	0.028	0.029
B(12)	−0.001	0.032	0.033	H(111)	−0.007	0.004	0.011
H(1)	−0.009	0.007	0.016	H(121)	−0.007	0.019	0.026
H(2)	−0.008	0.017	0.025	H(131)	−0.014	−0.006	0.008
H(5)	−0.078	−0.077	0.001	H(132)	−0.014	−0.004	0.010
H(6)	−0.073	−0.050	0.023	H(141)	−0.014	−0.007	0.007
H(7)	−0.102	−0.080	0.022	H(143)	−0.013	−0.002	0.011
H(8)	−0.107	−0.095	0.012	H(151)	−0.009	0.021	0.030
H(9)	−0.091	−0.097	0.006	H(161)	−0.013	−0.003	0.010
H(10)	−0.091	−0.083	0.008	H(171)	−0.013	−0.008	0.005
H(11)	−0.085	−0.075	0.010	H(172)	−0.014	−0.002	0.012
H(12)	−0.095	−0.098	−0.003	H(181)	−0.014	−0.005	0.009
				H(182)	−0.015	−0.002	0.013

gives selected interatomic distances and angles. In essence the structure of 4^+ is broadly similar to that of molecule **2**, but with the following important differences: (*i*) Pd(3) is significantly slipped (Δ = 0.22 Å) across the C_2B_3 face resulting in Pd–C_{cage} distances *ca.* 0.15 Å longer, on average, than Pd–B; at the same time the metallabonded C_2B_3 face is substantially less planar than that of **2** (σ = 0.122 and 0.047 Å, respectively); (*ii*) the observed conformation has α = 74.7°, which positions the C(15)–C(16) unit close to S and results in Pd–C(16) being substantially longer than Pd–C(15); and (*iii*) τ is −38.4° and the angle S–B(4)–B(8) is only 6.7° wider than S–B(4)–C(1). Thus, the measured conformation in 4^+ is not the expected one and, moreover, the usual orientation of the pendant SMe_2 group relative to C(1)H is not observed.

We believe that the overall stereochemistry of cation 4^+ *in the crystal* is substantially influenced by electrostatic interactions with adjacent BF_4^- anions, as detailed in Table 9. In particular we note that the closest inter-ion contact involves F(2′) and H(141) (one of the cod H atoms) which presumably has a non-trivial effect on the conformation in the cation, and that the second closest contact involves F(2″) and H(1), which presumably contributes to displacement of the (weak) S(lone pair)···H(1) bond.

Charge Distribution in Compounds **2** *and* 4^+.—As previously stated, 4^+ is an unusual example of a *cationic* heteroborane.[10,32] With only one exception[32a] all the previously reported cationic carbametallaboranes involve a function, bound to a cage boron atom, which could, in one extreme representation of the cation, be considered to carry the full positive charge. Indeed, molecular orbital calculations on the neutral compound $[Mn(CO)_3(SMe_2C_2B_9H_{10})]$[8] have previously suggested that here the S atom carries a charge of only +0.3e, implying that a degree of electronic flexibility is possible in ligands such as $SMe_2C_2B_9H_{10}$ and suggesting that much of the additional positive charge in cationic analogues could be accommodated on the pendant atom.

Compounds **2** and 4^+ constitute a pair of fully analogous (and structurally characterised) molecules that differ only in respect of the notional replacement of Rh^+ by Pd^{2+}. We have therefore performed fully charge-iterated EHMO calculations on the crystallographically determined models of them (with minimum ligand simplification, see Experimental section) to determine the distribution of the additional positive charge in 4^+. The results are summarised in Table 10.* Clearly, all atoms [with the trivial exceptions of H(5) and H(12)] are more positive in 4^+. The change at sulfur is only modest, +0.012e; rather the greatest single increase in positive charge occurs at the metal atom, +0.073e. Over all 12 cluster vertices there is an increase of +0.41e, with a further +0.34e being accommodated on the 'second sphere' atoms.

In broad terms, therefore, the results of these calculations show no substantial build up of positive charge at the pendant sulfur atom; rather they support the description of the cage of 4^+ as cationic.

* Confidence in the results of these calculations derives from the fact that the average increase in positive charge of cod C*H* and cage C*H* atoms is twice that of cod CH_2 atoms; we have already noted that the former atoms show substantially greater shifts to higher frequency in the ^{1}H NMR spectrum of 4^+ *cf.* that of **2**.

Acknowledgements

We thank the University of Edinburgh for a Dewar Studentship (to N. L. D.), the World Bank for financial support and the Callery Chemical Company and Drs. B. Stibr and J. Plesek for generous gifts of chemicals.

References

1 M. F. Hawthorne, *J. Organomet. Chem.*, 1975, **100**, 97.
2 R. N. Grimes, in *Comprehensive Organometallic Chemistry*, eds. G. Wilkinson, F. G. A. Stone and E. W. Abel, Pergamon, Oxford, 1981.
3 C. E. Housecroft, in *Specialist Periodical Reports in Organometallic Chemistry*, eds. E. W. Abel and F. G. A. Stone, Royal Society of Chemistry, London, 1991.
4 M. F. Hawthorne, D. C. Young and P. A. Wegner, *J. Am. Chem. Soc.*, 1965, **87**, 1818.
5 M. F. Hawthorne, D. C. Young, T. D. Andrews, D. V. Howe, R. L. Pilling, A. D. Pitts, M. Reintjes, L. F. Warren, jun. and P. A. Wegner, *J. Am. Chem. Soc.*, 1968, **90**, 879.
6 D. C. Young, D. V. Howe and M. F. Hawthorne, *J. Am. Chem. Soc.*, 1969, **91**, 859; E. H. S. Wong and M. F. Hawthorne, *Inorg. Chem.*, 1978, **17**, 2863; J. Plesek, Z. Janousek and S. Hermanek, *Collect. Czech. Chem. Commun.*, 1978, **43**, 2862; H. M. Colquhoun, T. J. Greenhough and M. G. H. Wallbridge, *J. Chem. Soc., Dalton Trans.*, 1979, 619; R. G. Teller, J. J. Wilczynsky and M. F. Hawthorne,

J. Chem. Soc., Chem. Commun., 1979, 472; R. E. King III, S. B. Miller, C. B. Knobler and M. F. Hawthorne, *Inorg. Chem.*, 1983, **22**, 3548; H. C. Kang, Y. Do, C. B. Knobler and M. F. Hawthorne, *J. Am. Chem. Soc.*, 1987, **109**, 6530; *Inorg. Chem.*, 1988, **27**, 1716.
7 E. J. M. Hamilton and A. J. Welch, *Acta Crystallogr., Sect. C*, 1990, **46**, 1228.
8 J. Cowie, E. J. M. Hamilton, J. C. V. Laurie and A. J. Welch, *J. Organomet. Chem.*, 1990, **394**, 1.
9 E. J. M. Hamilton and A. J. Welch, *Polyhedron*, 1991, **10**, 471.
10 E. J. M. Hamilton, Ph.D. Thesis, University of Edinburgh, 1990.
11 *Comprehensive Organometallic Chemistry*, eds. G. Wilkinson, F. G. A. Stone and E. W. Abel, Pergamon, Oxford, 1981.
12 J. A. McCleverty and G. Wilkinson, *Inorg. Synth.*, 1966, **8**, 211.
13 G. Giordano and R. H. Crabtree, *Inorg. Synth.*, 1979, **19**, 218.
14 D. A. White, *Inorg. Synth.*, 1972, **13**, 55.
15 CADABS, R. O. Gould and D. E. Smith, University of Edinburgh, 1986.
16 SHELX 76, G. M. Sheldrick, University of Cambridge, 1976.
17 DIFABS, N. G. Walker and D. Stuart, *Acta Crystallogr., Sect. A*, 1983, **39**, 158.
18 CALC, R. O. Gould and P. Taylor, University of Edinburgh, 1986.
19 SHELXTL, G. M. Sheldrick, University of Göttingen, 1985.
20 *International Tables for X-Ray Crystallography*, Kynoch Press, Birmingham, 1974, vol. 4, p. 99.
21 J. B. Casey, W. J. Evans and W. H. Powell, *Inorg. Chem.*, 1983, **22**, 2228.
22 ICON 8, J. Howell, A. Rossi, D. Wallace, K. Haraki and R. Hoffmann, Quantum Chemistry Program Exchange, University of Indiana, 1977, no. 344.
23 J. H. Ammeter, H.-B. Burgi, J. C. Thibault and R. Hoffmann, *J. Am. Chem. Soc.*, 1978, **100**, 3686.
24 D. L. Lichtenberger, C. H. Blevins II and R. B. Ortega, *Organometallics*, 1984, **3**, 1614.
25 J. Cowie, E. J. M. Hamilton, J. C. V. Laurie and A. J. Welch, *Acta Crystallogr., Sect. C*, 1988, **44**, 1648.
26 K. Wade, *Adv. Inorg. Chem. Radiochem.*, 1976, **18**, 1.
27 D. M. P. Mingos, M. I. Forsyth and A. J. Welch, *J. Chem. Soc., Dalton Trans.*, 1978, 1363.
28 D. M. P. Mingos, *J. Chem. Soc., Dalton Trans.*, 1977, 602.
29 N. Carr, M. C. Gimeno, J. E. Goldberg, M. U. Pilotti, F. G. A. Stone and I. Topaloglu, *J. Chem. Soc., Dalton Trans.*, 1990, 2253.
30 H. M. Colquhoun, T. J. Greenhough and M. G. H. Wallbridge, *J. Chem. Soc., Dalton Trans.*, 1985, 761.
31 J. Chatt and L. M. Venanzi, *J. Chem. Soc.*, 1957, 4735.
32 (*a*) R. J. Wilson, L. F. Warren, jun. and M. F. Hawthorne, *J. Am. Chem. Soc.*, 1969, **91**, 758; (*b*) M. F. Hawthorne, L. F. Warren, jun., K. P. Callahan and N. F. Travers, *J. Am. Chem. Soc.*, 1971, **93**, 2407; (*c*) C. J. Jones, J. N. Francis and M. F. Hawthorne, *J. Am. Chem. Soc.*, 1973, **95**, 7633; (*d*) H. C. Kang, S. S. Lee, C. B. Knobler and M. F. Hawthorne, *Inorg. Chem.*, 1991, **30**, 2024; (*e*) J. P. Sheehan, T. R. Spalding, G. Ferguson, J. F. Gallagher, B. Kaitner and J. D. Kennedy, *J. Chem. Soc., Dalton Trans.*, 1993, 35.

Received 8*th February* 1993; *Paper* 3/00761H